

## HIGH TEMPERATURE CREEP BEHAVIOUR OF RE-CONTAINING NICKEL-BASED SINGLE CRYSTAL SUPERALLOY

Chenguang Liu<sup>1</sup>, Zhijun Sun<sup>1</sup>, Yuan Li<sup>1</sup>, Zhengyu Yang<sup>1</sup>,  
Haiwen Wang<sup>1</sup>, Shuai Zheng<sup>1</sup>, Hao Zhao<sup>2</sup>

<sup>1</sup>Beijing Institute of Aeronautical Materials, P.R. China;

<sup>2</sup>China Electronic Product Reliability and Environmental Testing Research Institute, P.R. China  
chenguang.liu@biam.ac.cn , zhijun.sun@biam.ac.cn , zhenyu.yang@biam.ac.cn ,  
haiwen.wang@biam.ac.cn , shuai.zheng@biam.ac.cn , zhaohao1@ceprei.com

**Abstract.** Microstructure evolution of creep behaviours and the rupture mechanism of a nickel-based single crystal superalloy containing 3% Re under 1070 °C/140MPa were studied systematically. Three stages can be divided as primary, steady and accelerated stages. Raft structure formed and dislocations aggregated in  $\gamma/\gamma'$  phase interfaces in the primary stage. Raft structure coarsens and topological inversion occurs, and dislocation network exhibits quadrilateral structure in the steady creep stage. Raft structure continues to coarsen and de-raft in the accelerated stage. High temperature creep process is a mixed fracture mode with aggregated micropores and local plastic deformation.

**Keywords:** single crystal superalloy,  $\gamma/\gamma'$  phase structure, creep, rafting, dislocation network.

### Introduction

Nickel-based single crystal superalloy is a key material for advanced aero-engine turbine blades due to its excellent high-temperature mechanical properties [1]. The nickel-based single crystal alloy in turbine blades undergoes rafting during service and its microstructural variation affects its mechanical properties seriously [2; 3]. Caron et al. [4] summarized the influence of raft organization on creep performance and thought that lateral climbing and slippage of the  $a/2 \langle 011 \rangle$  interfacial dislocations at the  $\gamma/\gamma'$  phase interface is the dominant mechanism in the steady-state creep stage. Rafted structure increases the resistance of the dislocation movement, which is beneficial to its creep performance. Studies show that the high density of dislocation networks in the steady creep stage can hinder the dislocations climbing and prevent further cutting into the  $\gamma'$  phase. The greater the degree of mismatch between the  $\gamma$  and  $\gamma'$  phases, the stronger the ability to block dislocation climbing [5]. Reed et al. [6] believed that a rafted structure hindered climbing and slippage of  $a/2 \langle 110 \rangle \{111\}$  dislocations and deformation will form creep holes by further creep. In the accelerated creep stage, the alloy exhibits a rapid increase in the amount of creep strain and creep rate. However, there are still different opinions on the rapid increase in the creep rate. Epishin et al. [7] believed that the topological inversion of the  $\gamma/\gamma'$  phase structure was mainly attributed to fast creep rate.

Therefore, it is necessary to study the creep behaviour of nickel-based single crystal superalloys. The creep behaviour of a second-generation single crystal superalloy containing Re 3% at 1070 °C/140MPa will be studied in this paper to clarify the creep rupture mode, microstructure evolution and deformation mechanism. The study provides ideas for further optimization of the composition design and improvement of the mechanical properties of superalloys.

### Experiment

The material used in this study is a second-generation single-crystal superalloy with nominal composition (wt.%) is Cr(4.0), Co(8.0), Mo(2.0), W(7.0), Re(3.0), Ta(7.0), Nb(0.5), Al(6.0), Hf(0.2), Ni(bal). The spiral crystal selection method is used to prepare single crystal test bars in the HRS directional solidification furnace, and the as-cast alloy is subjected to solid solution and aging heat treatment. The specific system is 1290 °C/1 h + 1300 °C/1 h + 1310 °C/2 h + 1318 °C/6 h (air cooling), 1130 °C/4 h (air cooling), 870 °C/32 h (air cooling).

The creep test runs under the condition of 1070 °C/140MPa and the sample as fabricated, Fig. 1. FEI-Nova Nano SEM 450 type field emission scanning electron microscope and JEM-2010 type transmission electron microscope were used for observation.

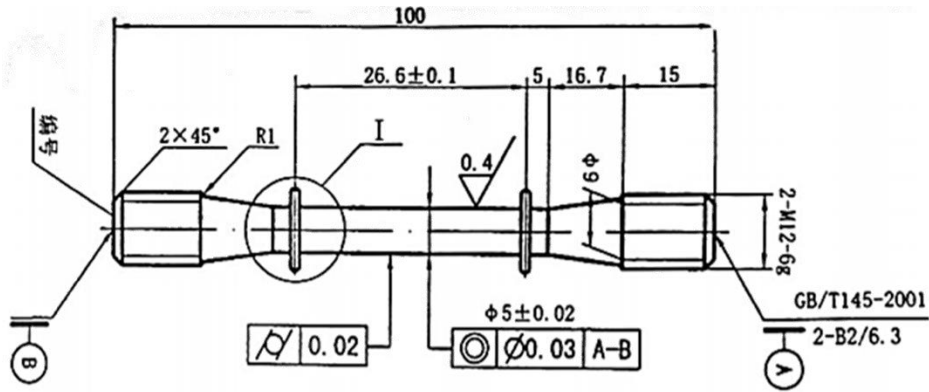


Fig. 1. Demonstration of test samples

## Result

Fig. 2a-b shows the creep stress-time and stress-strain curves of the alloy at 1070 °C/140 MPa. The stress-time curve shows that the alloy's creep life is 316.20 h, showing typical three-stage creep characteristics, namely, the primary stage, steady-state stage and accelerated stage. The stress-strain curve shows that the strain rate firstly decreases and then increases, indicating that there is a deformation hardening and softening process.

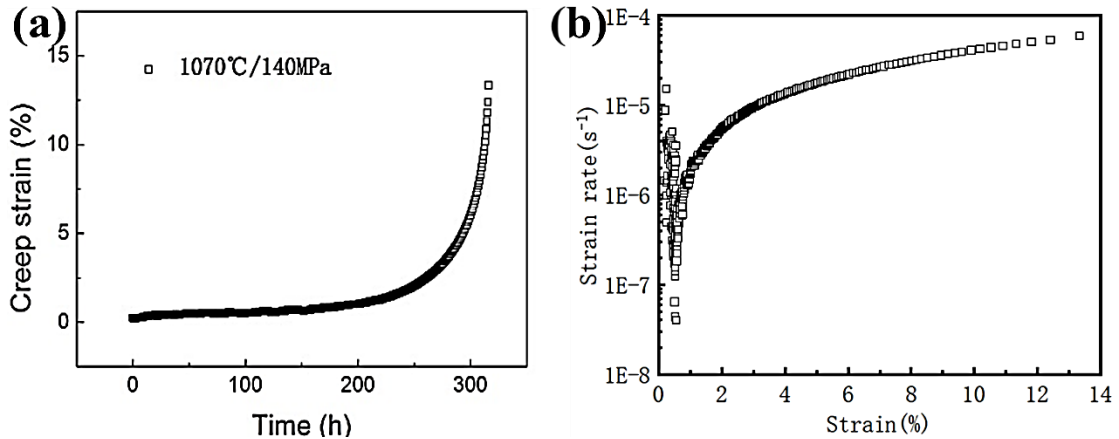


Fig. 2. Creep test curve at 1070 °C/140 MPa: a – Stress-time curve; b – Strain rate-strain curve

Fig. 3a-f shows the evolution of the  $\gamma/\gamma'$  phase morphology of the alloy at different stages. At the beginning of creep, the horizontal channel is coarsened, while the  $\gamma'$  phase expands toward the horizontal direction. As creep goes on, the vertical channels almost disappear, and the horizontal channels continue to coarsen. The decrease of the  $\gamma'$  phase width is caused by the directional diffusion of the  $\gamma'$  phase forming elements Al, Ti, and Ta. When the creep reached the steady-state stage for 100 h, the rafting process finished, and the connection nodes of the matrix channel networks in the horizontal direction decreased. When the creep time reaches to 200 h, the raft structure keeps stable, while the  $\gamma$  phase is transformed from the interconnected network to separated parallel channels. It forms a “Topological Inversion” structure defined by Fredholm et al. [8] that the morphology of the matrix phase and the strengthening  $\gamma'$  phase reverse. In the accelerated stage, the  $\gamma$  phase evolves to short ribbons, and topological inversion accelerates. Near the creep rupture nick, the straight raft structure disappears, and the interface between the two phases is no longer perpendicular to the stress axis, which suggests that the raft structure is unstable and de-rafted process occurred [9].

Fig. 4 shows the evolution of dislocations and interfacial dislocation networks during creep. It can be seen from Fig. 2a-e that at the end of the primary creep stage, lots of dislocations are generated located in the  $\gamma/\gamma'$  phase interface, and aggregated in the interface. In the primary stage, the dislocations can move into the channel of the  $\gamma$  matrix only if the applied stress and internal mismatch stress are sufficient to overcome the Orowan obstruction in the lateral channel of the  $\gamma$  matrix. As the creep goes on, the  $\gamma$  matrix channel widens, resulting in a decrease of Orowan resistance [10].

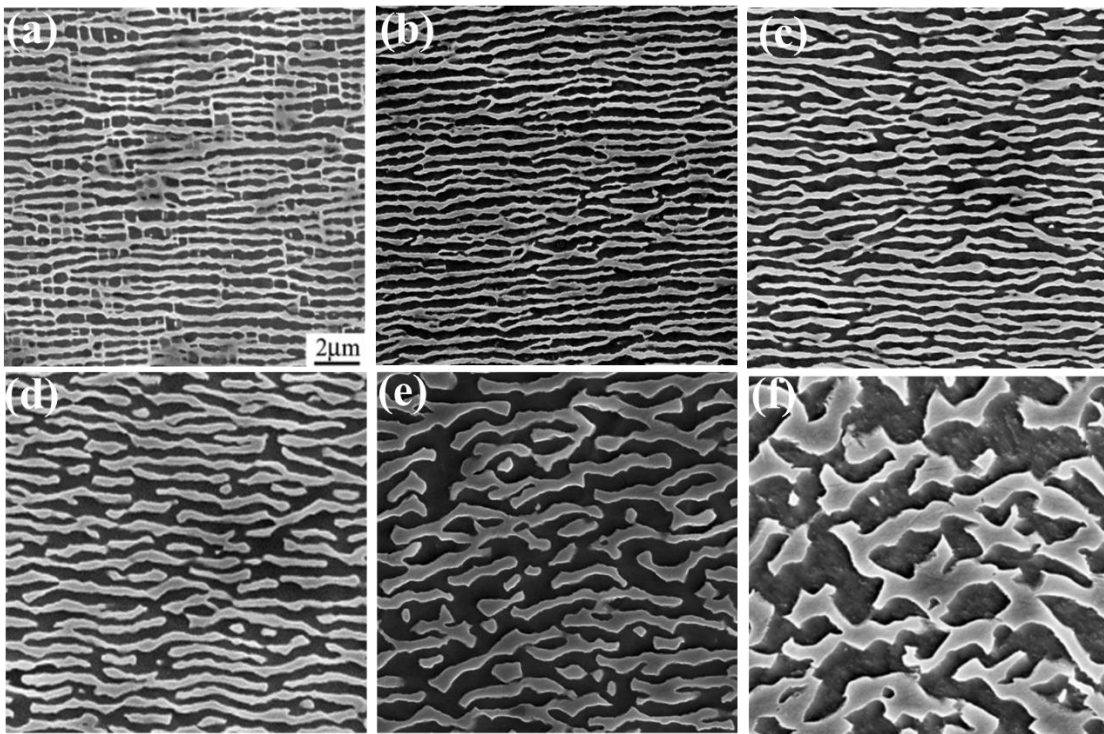


Fig. 3. Evolution of  $\gamma/\gamma'$  phase morphology during creep at 1070 °C/140 MPa:  
a – 5h; b – 20h; c – 100 h; d – 200 h; e – 300 h; f – near the rupture

It is more conducive for the movement of dislocations in the matrix channel which leads to an accelerated creep strain rate. As the creep deformation increases, some dislocations will accumulate at the phase interface, resulting in a decrease of the creep strain rate and a release of the interface mismatch stress. Then the  $\gamma'$  phase begins to form a rafted structure. In the steady-state creep stage, the distance between the dislocation lines decreases continuously as shown in Fig. 4b, and the interface dislocations of different slip systems in the matrix begin to react under the interaction of the stress field to finally form dislocation network structure. At the initial stage of steady creep, nearly no dislocations were found in the  $\gamma'$  phase as shown in Fig. 4b, while at the end of the steady creep, there were several dislocations cutting into the  $\gamma'$  phase. It means that dislocation cutting  $\gamma'$  phase is the main deformation mechanism in the steady creep stage. Studies [11] shows that this type of dislocation is an antiphase domain boundary with a significant obstruction on the slip of the dislocation, resulting in a lower steady creep rate. In addition, the density of the dislocation network at the interface gradually increases at this stage. The presence of a quadrilateral dislocation network can be observed at the end of the steady-state creep stage [12-13], which hinders climbing other structures since they are formed by the quadrilateral through the dislocation reaction. The increase of the dislocation network density and the existence of the quadrangular dislocation network both result in a low creep rate.

The creep fracture morphology is shown in Fig. 5a. The end face is round without obvious macroscopic crystallographic orientation. As shown in Fig. 5b, there is a small plane morphology in part of the rupture area as the propagation path of the crack initiating at the centre micro hole. The creep cavity surfaces tend to be parallel to the crystal orientation with lower interfacial energy, such as {110} plane, making the pores become a polyhedron as shown in Fig. 5d. As the creep progresses, the micropores gather together and grow into large pores, causing stress concentration in local areas until they exceed the yield stress. The coarsened structure will then be plastically deformed, which further reduces the load cross-sectional area, causes the propagation and connection of the crack and eventually leads to creep rupture. Therefore, the rupture mode of alloy under high temperature creep is a mixed rupture mode characterized by micro-hole aggregation and local plastic deformation. In this study, the creep rate did not increase rapidly with the topological inversion during the accelerated creep stage. However, as the creep continues, the integrity of the dislocation network is reduced in Fig. 5f, and the local stress concentration causes a large number of dislocations to cut the  $\gamma'$  phase movement and it is the main reason for the rapid increase of accelerated creep stage.

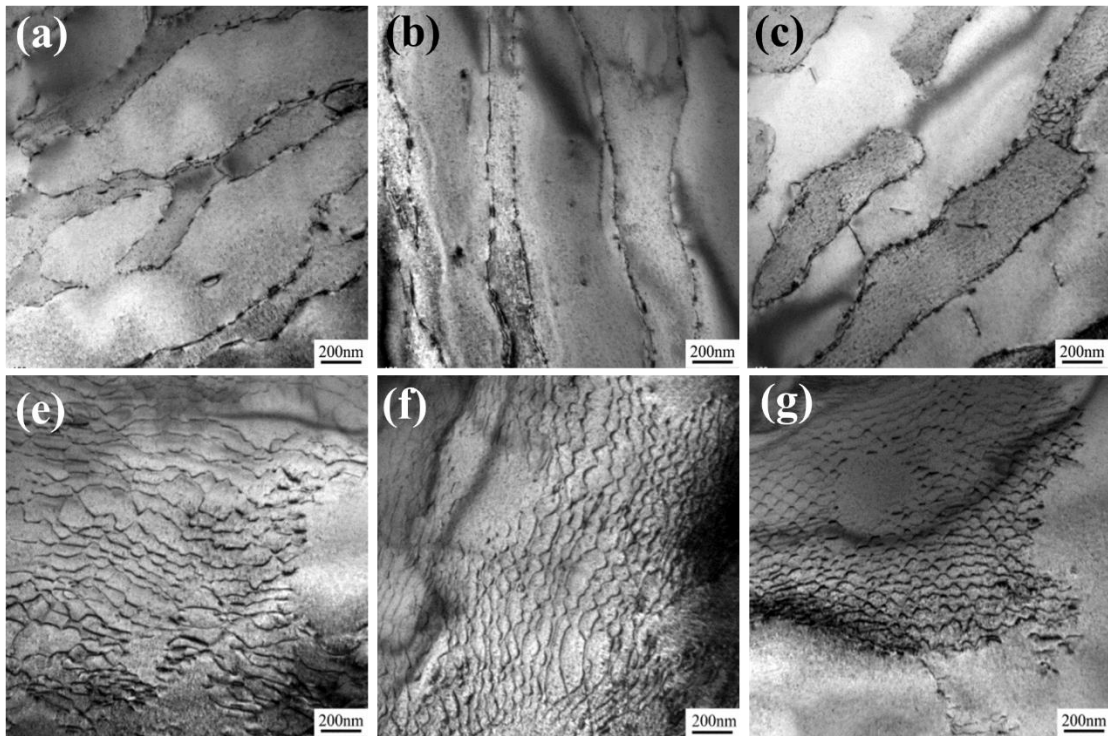


Fig. 4. Evolution of interface dislocation network during alloy creep:  
a, e – 20h; b, f – 100h; c, g – 200h; B = [001], g = 002

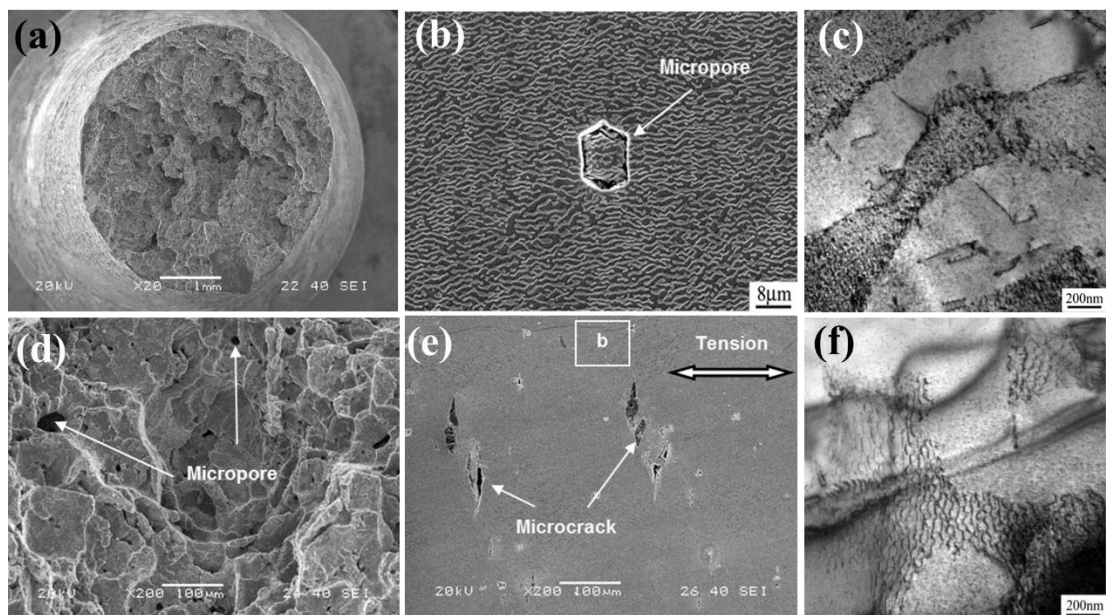


Fig. 5. SEM images on creep rupture: a, d – crack morphology; b, e – magnified micropores;  
c, f – TEM images on dislocations in longitudinal section

## Conclusions

Microstructure evolution of creep behaviours and the rupture mechanism of a single crystal superalloy containing 3% Re under 1070 °C/140 MPa were studied systematically. The creep process contains three stages: the first stage contains the structure rafting fast and dislocations aggregate in  $\gamma/\gamma'$  phase interfaces, in the second stage the raft structure coarsens and topological inversion occurs, and the third stage contains the de-rafting process. A mixed fracture mode with aggregated micropores is the main microstructure for high temperature creep process and local plastic deformation.

### Author contributions

Experiment, Y.Z.; methodology, H.W.; formal analysis, G.Y.; investigation, S.Z.; writing – original draft preparation, Q.W.; writing – review and editing, C.L. and B.S. All authors have read and agreed to the published version of the manuscript.

### Conflicts of interest

The authors declare no conflict of interest.

### Acknowledgments

This work was supported by the Natural Science Foundation of China (Nos. 52001297, 91860202).

### Reference

- [1] Reed RC. The Superalloy Fundamentals and Applications. Cambridge University Press London: 2016.
- [2] Yunsong ZJ, Zhang F, et al. Effect of trace boron on microstructural evolution and high temperature creep performance in Re-containing single crystal superalloys. *Progress in Natural Science. Materials International*: v.30(03), 2020, pp. 97-107.
- [3] Kamaraj M. Rafting in single crystal nickel-base superalloys. An overview. *Sadhana*: 28(1), 2003, pp. 115-128.
- [4] Caron P, Henderson P J, Khan T, et al. On the effects of heat treatments on the creep behaviour of a single crystal superalloy. *Scripta metallurgica*: 20(6), 1986, pp. 875-880.
- [5] Zhang J X, Wang J C, Harada H, et al. The effect of lattice misfit on the dislocation motion in superalloys during high-temperature low-stress creep. *Acta Materialia*: 2005.
- [6] Matan N, Cox D C, Rae C, et al. On the kinetics of rafting in CMSX-4 superalloy single crystals. *Acta Materialia*: 47(7), 1999, pp. 2031-2045.
- [7] Epishin A, Link T. Mechanisms of high-temperature creep of nickel-based superalloys under low applied stresses. *Philosophical Magazine*: 84(19), 2004, pp. 1979-2000.
- [8] Fredholm A, Strudel J L. High Temperature Creep Mechanisms in Single Crystals of Some High Performance Nickel Base Superalloys. Springer Netherlands: 1987.
- [9] Nathal M V, Ebert L J. Gamma prime shape changes during creep of a nickel-base superalloy. *Scripta Metallurgica*: 17(9), 1983, pp. 1151-1154.
- [10] Pollock T M, Argon A S. Overview no. 95 creep resistance of cmsx-3 nickel base superalloy single crystals. *Acta Metall. Mater*: 40(1), 1992, pp. 1-30.
- [11] Linka T, Epishin A, Klaus M, Brückner U, Reznicek A.  $\langle 100 \rangle$  Dislocations in nickel-base superalloys: Formation and role in creep deformation - ScienceDirect. *Materials Science and Engineering A*: 405(1-2), 2005, pp. 254-265.
- [12] An N, Sun Y, Wu Y, et al. High temperature strengthening via nanoscale precipitation in wrought CoCrNi-based medium-entropy alloys. *Materials Science and Engineering A*: 798(19), 2020, 140213.
- [13] Feng Y, Zhou X, Zou J, et al. Effect of Inclusions on Low Cycle Fatigue Lifetime in Powder Metallurgy Superalloy FGH96. *Rare Metals*: 7, 2021, 2455.